Lasers Med Sci (2007) 22:143–157
DOI 10.1007/s10103-006-0430-x

ORIGINAL ARTICLE

Er:YAG laser therapy for peri-implant infection: a histological study

Aristeo Atsushi Takasaki · Akira Aoki · Koji Mizutani · Shigenari Kikuchi · Shigeru Oda · Isao Ishikawa

Received: 26 September 2006 / Accepted: 22 November 2006 / Published online: 12 January 2007

Abstract The purpose of this study was to evaluate the effects of Er:YAG laser on degranulation and implant surface debridement in peri-implant infection. The peri-implant infection was experimentally induced in dogs, and the treatment was performed using an Er:YAG laser or a plastic curet. Animals were sacrificed after 24 weeks, and undecalcified histological sections were prepared and analyzed. Degranulation and implant surface debridement were obtained effectively and safely by Er:YAG laser. Histologically, a favorable formation of new bone was observed on the laser-treated implant surface, and the laser group showed a tendency to produce greater bone-to-implant contact than the curet group. These results indicate that the Er:YAG laser therapy has promise in the treatment of peri-implantitis.

Keywords Animals · Er:YAG laser · Granulation tissue · Histometrical analysis · Implant debridement · Peri-implantitis · Surgery

Contract grant sponsor: 21st Century Center of Excellence Program for Frontier Research on Molecular Destruction and Reconstruction of Tooth and Bone in Tokyo Medical and Dental University and a Grant-in-Aid for Scientific Research(c)(2) (No. 16592064) (A.A.), Ministry of Education, Culture, Sports, Science and Technology of Japan.

A. A. Takasaki (✉) · A. Aoki (✉) · K. Mizutani · S. Kikuchi · S. Oda
Section of Periodontology,
Department of Hard Tissue Engineering, Graduate School,
Tokyo Medical and Dental University,
1-5-45 Yushima, Bunkyo-ku,
Tokyo 113-8549, Japan
e-mail: arisperi@tmd.ac.jp
e-mail: aoperi@tmd.ac.jp

A. A. Takasaki
21st Century Center of Excellence Program for Frontier Research on Molecular Destruction and Reconstruction of Tooth and Bone,
Tokyo Medical and Dental University,
Tokyo, Japan

I. Ishikawa
Tokyo Medical and Dental University,
Tokyo, Japan

I. Ishikawa
Institute of Advanced Biomedical Engineering and Science,
Tokyo Women's Medical University,
Tokyo, Japan

Introduction

Lasers apparatus have been recently applied for the treatment of oral diseases. It is well established that the Erbium-doped:Yttrium–Aluminum–Garnet (Er:YAG) laser, emitting at a wavelength of 2.94 μm, possesses suitable properties not only for soft tissue therapy but also for hard tissue treatment due to its characteristic wavelength that is highly absorbed by water [1]. Recently, in periodontics, several in vitro studies demonstrated the effectiveness of Er:YAG laser application for the removal of subgingival calculus [2–5]. Our recent animal study demonstrated an effective and safe application of the Er:YAG laser for granulation tissue removal and root surface debridement and the promotion of new bone formation in periodontal surgery procedures [6].

Peri-implantitis has been classified as an inflammatory process affecting an osseointegrated implant in function, resulting in a loss of supporting bone. The disease is closely associated with specific microorganisms known collectively as periodontopathic bacteria [7, 8], and a number of surgical and nonsurgical therapeutic strategies to treat peri-implantitis have been studied [9–14].

Recently, various lasers have been introduced as a novel technical modality for the treatment of peri-implantitis, and promising results have been reported [12, 14–16]. With the Er:YAG laser, it has been demonstrated that the effective removal of calculus and plaque on contaminated abutments is possible under suitable irradiation parameters without titanium surface damage or major temperature elevation [17]. Considering the results of previous studies [18, 19] and the advantageous properties of the Er:YAG laser in periodontal therapy, such as excellent tissue ablation [2–6] with high bactericidal [20, 21] and detoxification effects [22, 23], the potential of Er:YAG laser application for the treatment of peri-implantitis would be expected [24–26]. The purpose of this study was to compare the effectiveness of Er:YAG laser therapy for granulation tissue removal and implant surface debridement in the treatment of peri-implant infection and to histologically evaluate the ensuing bone healing with those of conventional mechanical debridement using a plastic curet.

Materials and methods

Animals

Four healthy 1-year-old beagle dogs (average body weight 12.0 kg) were used in this study. The animals exhibited intact dentition with a healthy periodontium. The protocol design and procedures of animal experiment were approved by the ethical committee of Animal Research Center of Tokyo Medical and Dental University.

Laser apparatus

The laser apparatus applied was an Er:YAG Laser (DE-Light™, HOYA Conbio, Fremont, CA, USA). The features of this apparatus were: wavelength 2.94 μm, an output energy range of settings from 30 to 350 mJ/pulse, a maximum pulse repetition rate of 30 pulses per second (Hz), and a pulse duration of 200 μs. The apparatus employed an optical fiber delivery and contact probe system. In this study, a chisel tip (P/N 625-8746) made of sapphire glass, with a rectangular pointed head of 1.40× 0.45 mm dimension and approximately 82% laser transmission (a brand new chip) was used in a contact mode. The energy level of the laser irradiation was determined by measuring the output power at the end of the contact tip using a power meter (Field Master™, Coherent, Santa Clara, CA, USA). The laser apparatus also uses a special water spray system to cool the irradiated area. Air-mixed water was released coaxially to the contact tip covering the target during the irradiation. This water spray system provides precise and adequate water delivery. An optional feed bottle system was integrated in the apparatus for the supply of sterile physiological saline solution during irradiation.

Surgical protocol

All surgical procedures were performed under general and local anesthesia under aseptic conditions. Medetomidine hydrochloride (Dormitor®, Orion, Espoo, Finland, 0.05 ml/kg) was administered intramuscularly as a premedication. General anesthesia was achieved using an intravenous sodium thiopental (RAVONAL® Tanabe, Osaka, Japan, 0.005 ml/kg) injection. Additional sodium thiopental was injected to maintain anesthesia throughout the surgical procedure. Local anesthesia was performed with the injection of 2% lidocaine hydrochloride containing epinephrine at a concentration of 1:80,000 (Xylocain® Cartridge for Dental Use, Fujisawa, Osaka, Japan). The animals were fed a soft consistency laboratory diet (DKM®, Oriental Yest, Tokyo, Japan) throughout the study. A soft diet was chosen to reduce the chance of mechanical interference with healing during food intake.

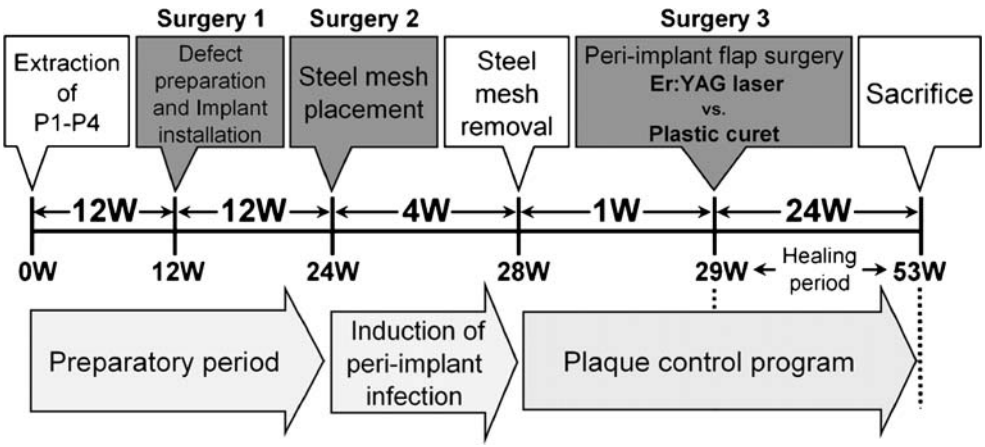

Fig. 1 Outline of the experiment

Defect preparation and implant placement

At the beginning of the experiment, as shown in Fig. 1, all mandibular premolars (P1–P4) were extracted bilaterally. Twelve weeks later, implants were placed. After alveolar crest incision, mucoperiosteal flaps were elevated in the edentulous mandibular premolar regions. The irregular alveolar crest was planed using a steel bur, and the implant beds with a buccolingual thickness of approximately 5–6 mm were prepared. Then, on each side, two access holes were drilled by stepwise enlargement with physiologic saline cooling. Before fixture installation, a buccal dehiscence-type defect, approximately 5 mm in height from the crestal bone and 3 mm in width mesiodistally, was prepared with a straight fissure steel bur for each access hole (Fig. 2a and d). The defect size was standardized with a periodontal probe (PCPUNC 15, Hu-Friedy, IL, USA). Following defect preparation, two Sand-blasted Large grit Acid-etched (SLA) surface implants (solid screw ø 3.3×10 mm standard plus, ITI® Dental Implant System, Straumann AG, Waldenburg, Sweitzerland) were placed in each side (Fig. 2b and e). Subsequently, vinyl polysiloxane impression material (EXAFINE® REGULAR, GC, Tokyo, Japan) was injected into the bone defect in direct contact with the exposed implant surface to prevent spontaneous bone healing during implant osseointegration (Fig. 2c and f). Following surgery, the periosteum of the flaps were fenestrated for relaxation, and the extended flaps were repositioned to completely submerge the implants and were closed using vertical mattress and interrupted sutures (GORE-TEX® CV-5 Suture, W.L. Gore and Associates, Flagstaff, AZ, USA). All implant placements were performed by the same operator (S.K.) according to the manufacturer's protocol. Following implant installation, the dogs received antibiotics (Penicillin G, 200,000 U/day) and analgesics (Butorphanol tartrate, 2 mg/ml) intramuscularly, and a clinical plaque control using a 2% solution of chlorhexidine gluconate (5% HIBITANE® concentrate, Sumitomo, Osaka, Japan) was performed three times a week for the following period until the next surgical therapy.

Induction of peri-implant infection

Three months after implant installation, the induction of peri-implant infection was initiated. After mucoperiosteal flaps reflection, the silicone impression material placed in the buccal bone defect (Fig. 3a) was removed and a healing abutment (4.5 mm length) was placed in each implant (Fig. 3b). To induce peri-implant infection in the bone defect and contaminate the exposed implant surface while simultaneously allowing the formation of diseased granulation tissue, a stainless steel mesh sheet (12×2.7 mm)

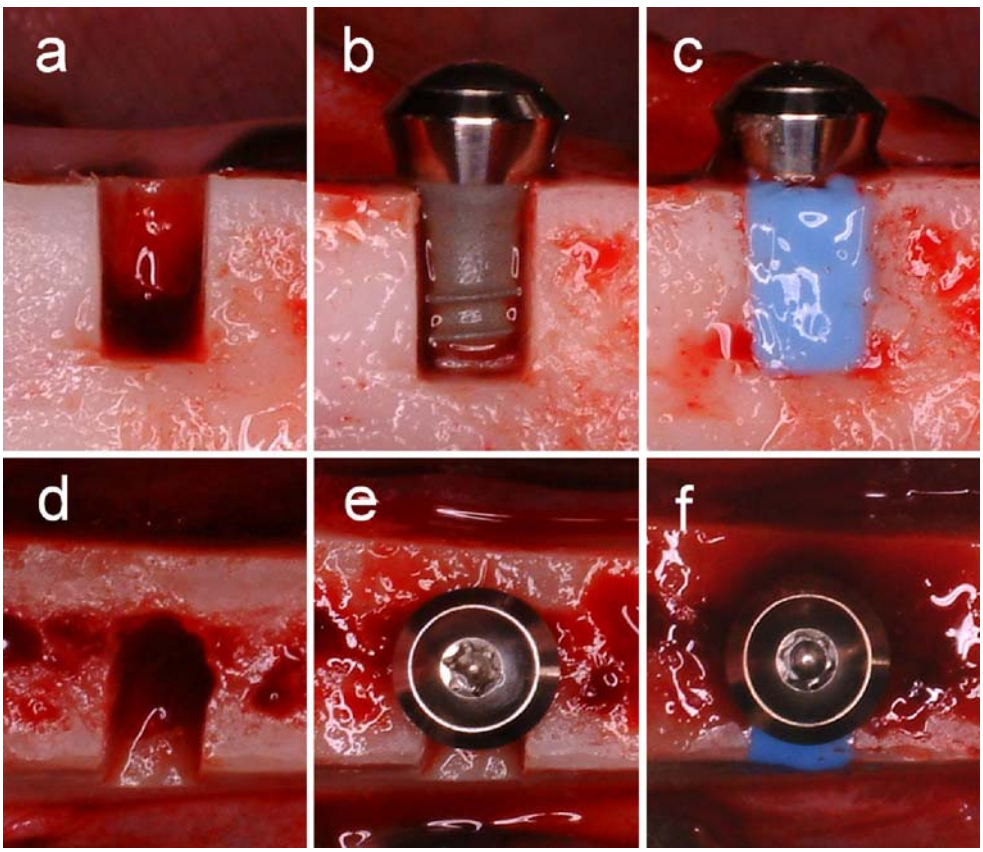

Fig. 2 The series of defect preparation and implant placement procedures. Twelve weeks after extraction of P1–P4, a dehiscence-type defect, 5 mm in height and 3 mm in width, was surgically created in the buccal aspect of each drilled implant hole (**a**), and then, an implant fixture was placed in such a way that the border line between the intra-osseous and the transmucosal portion of the implant coincided with the level of the bone crest (**b**), and then, the buccal bone defect was filled with silicone impression material to maintain the shape of the original bone defect by preventing spontaneous bone healing during implant osseointegration (**c**). Occlusal views of the site: implant hole with the buccal defect (**d**), after implant placement (**e**), and after silicone filling (**f**)

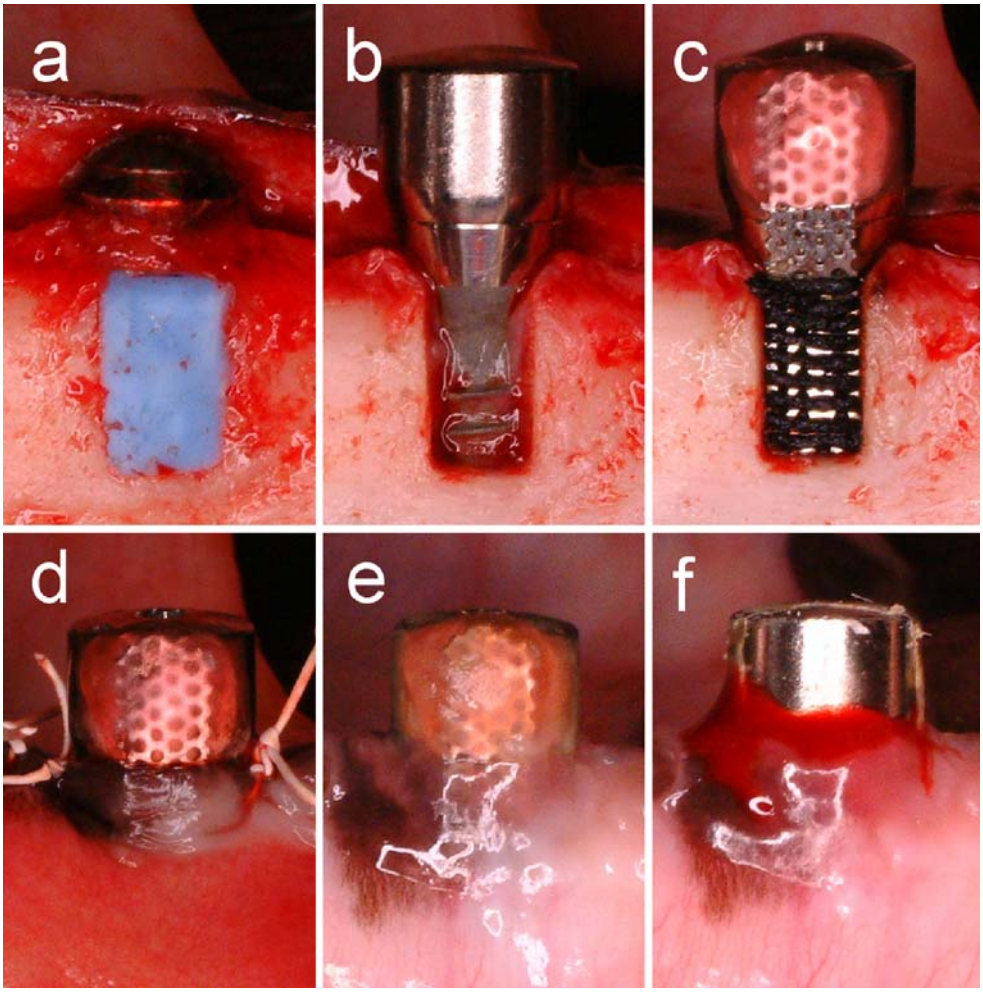

Fig. 3 The series of procedures for induction of experimental peri-implant infection. Full thickness flaps were elevated (**a**), and after removal of the silicone, healing abutment was placed (**b**). Then, stainless steel mesh with silk ligature was placed into the defect and fixed to the healing abutment for the induction of the infection and simultaneously allowing the formation of diseased granulation tissue (**c**). Flaps closed (**d**). Supragingival plaque and calculus accumulation and signs of gingival inflammation were observed after 4 weeks of infection (**e**). After nonsurgical removal of the steel mesh, an abundant spontaneous bleeding from the pocket of the defect site was observed (**f**)

(TOMY Bonding Base M®, TOMY, Tokyo, Japan) with a silk ligature (ø 0.15–0.19 mm) was placed into the defect and fixed on the healing abutment using an adhesive resin cement (Super Bond C&B® SUN MEDICAL, Shiga, Japan) after roughening the abutment surface with a silicon carbide bur and acid-etching (Fig. 3c). The flaps were repositioned and sutured (Fig. 3d). From the date of the mesh placement to the fourth week, no oral hygiene procedures were performed.

After 4 weeks of the steel mesh sheet placement, the presence of supragingival plaque and calculus were confirmed around the implant (Fig. 3e), and the steel mesh was carefully removed nonsurgically. Signs of gingival inflammation were noted in the buccal side of the implant, and spontaneous bleeding was observed from the peri-implant pocket after mesh sheet removal (Fig. 3f). The presence of submarginal plaque attached to the silk ligature of the contaminated metal mesh was also observed. The chemical plaque control previously described was reestablished.

Bacterial detection by PCR

Immediately after removal of the steel mesh in one dog, submarginal dental plaque sample was collected from the silk ligature on the contaminated steel mesh using sterile paper points to examine the infection of periodontopathic bacteria in the peri-implant pocket. Bacterial detection by polymerase chain reaction (PCR) was performed to identify five major periodontopathic bacteria [*Actinobacillus actinomycetemcomitans* (*A.a.*), *Porphyromonas gingivalis* (*P.g.*), *Prevotella intermedia* (*P.i.*), *Tannerella forsythia* (*T.f.*), and *Treponema denticola* (*T.d.*)] in submarginal plaque. The paper point with the plaque sample was kept in sterilized plastic tube, and 1 ml of sterile distilled water was added and mixed for 1 min by vortex. After removing the paperpoint, each sample was collected by centrifuge at 10,000 rpm for 5 min. The resulting pellet was resuspended in 200 µl of sterile distilled water and then heated at 100°C for 10 min. The supernatant of each sample was used as the template for PCR. According to the method described by

Ashimoto et al. [27], the design and specificity of primers were selected, and PCR analysis was performed.

Surgical therapy of peri-implant infection

After 1 week of mesh removal, the acute inflammation was reduced, and the surgical treatment of the experimentally induced peri-implant infection was carried out. Under general and local anesthesia, intracrevicular incisions and full thickness flap elevation were performed, and the buccal diseased lesion with peri-implant infection was exposed (Fig. 4a and c). On the implants on the right side (experimental side), granulation tissue removal and implant surface debridement were performed by means of only Er:YAG laser irradiation without any other mechanical instrumentation. The Er:YAG laser irradiation was carried out under sterile saline water spray in direct contact with implant and bone surface by maintaining the contact tip oblique to the implant surface at an angle of approximately 30–45° in a scraping motion from top to bottom (Fig. 4b). The actual energy output was selected as 62 mJ/pulse (approximately 95–105 mJ/pulse on the panel) which was equivalent to an energy density of 10.0 J/cm^2 per pulse at the end of the contact tip. The pulse repetition rate employed was 20 Hz. These parameters were determined according to our previous study [6, 17] and pilot experiments (data not shown). On the implants placed on the left side (control side), granulation tissue removal and implant surface debridement was performed by plastic curet (IMPLACARE™, Hu-Friedy, Chicago, IL, USA) as a control (Fig. 4d). After debridement with the curet, the titanium surface was meticulously cleaned with copious physiological saline solution irrigation. The endpoint of debridement for each treatment was determined by macroscopic inspection of the defect site. Each time period required for laser irradiation or mechanical instrumentation was measured, not including the time for tip adaptation and inspection of the residual granulation tissue. Also, the degree of difficulty of treatment (A: very easy, B: easy, C: difficult, and D: impossible) and the degree of bleeding from the bone defect after debridement (A: excessive, B: moderate, C: slight, and D: no) were scored in both groups.

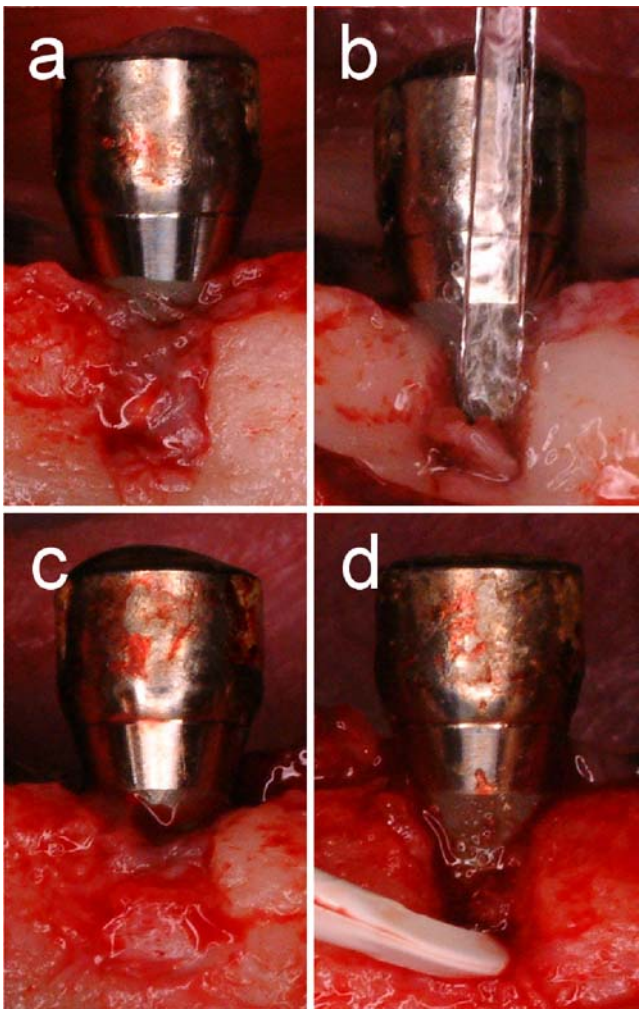

Fig. 4 Operative view of the surgical therapy procedures of experimentally induced peri-implant infection. After elevation of the mucoperiosteal flap, the bone defects were exposed. The bone tissue adjacent to the defect had been resorbed to some extent, and the defects were filled with diseased connective tissue (**a**, **c**). In the laser sites, degranulation and implant surface debridement were performed with Er:YAG laser irradiation under sterile water spray in contact mode by maintaining the chisel tip (rectangular pointed head of 1.40× 0.45 mm) at an angle of approximately 30–45° to the implant and bone surface in a scraping motion from top to bottom at an energy density of approximately 10.0 J/cm^2/pulse and a pulse rate of 20 Hz (**b**). In the control sites, granulation tissue removal and implant surface debridement was performed by plastic curet, and then, the titanium surface was meticulously cleaned with copious physiological saline solution irrigation (**d**)

After debridement of the bone defect, a photograph of the buccal horizontal view of the defect with a periodontal probe placed vertically in the center of the defect was taken to determine the position of the bottom and the height of the defect for the following histometrical analysis (Fig. 5a). After the procedure, the periosteums of the buccal and lingual flaps were fenestrated for flap relaxation, and the extended flaps were repositioned to completely cover and submerge the implants. All the procedures for the induction of peri-implant infection and both flap surgeries in all dogs were performed by one experienced operator (A.A.).

All dogs received analgesic following surgery and antibiotics for 3 days postsurgery. Sutures were removed after 2 weeks. The chemical plaque control previously described was continued until sacrifice. During the healing phase, for the implants exposed from the mucosa, chemical, and mechanical supragingival implant, cleaning was additionally performed once a month.

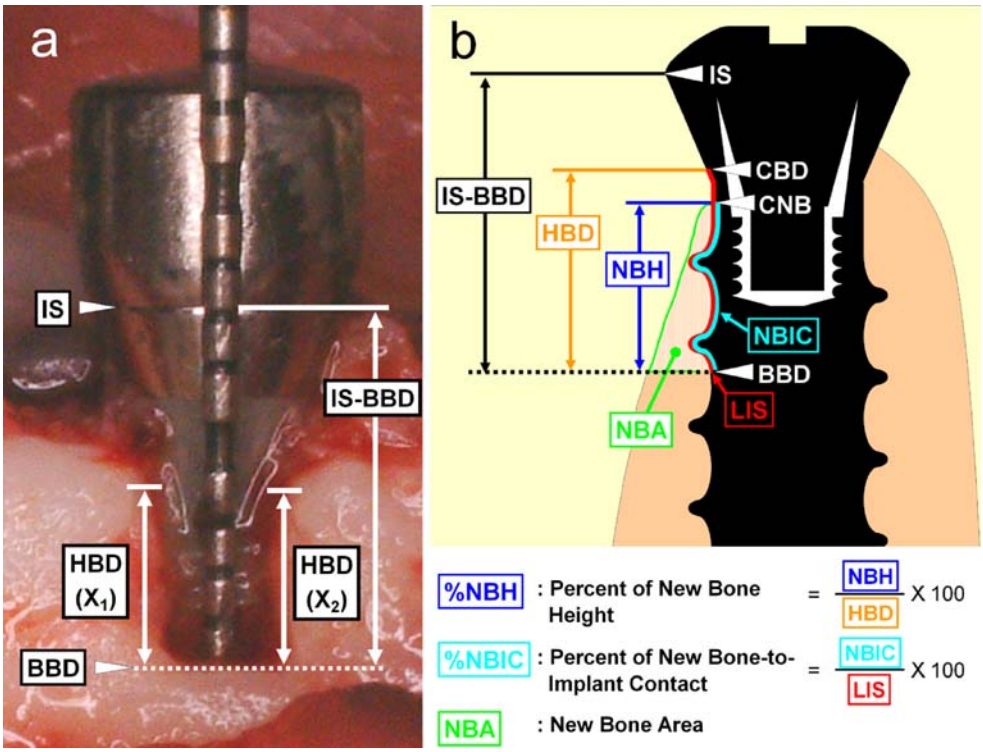

Fig. 5 Schematic photograph and illustration showing the *landmarks* used for histometrical evaluation. Photograph of the buccal horizontal view of the defect with a periodontal probe placed vertically in the center of the defect to determine the distance between the implant shoulder to the bottom of the defect (*IS-BBD*). The distances between the most coronal part of both the mesial (X_1) and distal (X_2) buccal alveolar crest of the bone defect and the bottom of the defect were measured, and the mean of both distances was determined and designated as the height of the bone defect (*HBD*) (**a**). Schematic drawing of the histometrical measurements analyzed in the buccolingual histological sections. After determining *BBD*, the area of newly formed bone (*NBA*), the percent of new bone height (*NBH*) to *HBD* (*%NBH*), and the percent of new bone-to-implant contact (*NBIC*) to total length of implant surface within the original bone defect (*LIS*) (*%NBIC*) were measured and calculated for each histological section (**b**). *IS* Implant shoulder, *BBD* bottom of the bone defect, *CBD* coronal level of bone defect, *CNB* Coronal level of newly formed bone

Histological processing

Twenty-four weeks after surgery, the animals were sacrificed with an overdose of sodium thiopental. Following the perfusion fixation of the head and neck with 10% buffered formalin, the mandibles were removed and block sections of each implant site on the experimental and control sites were dissected with the surrounding soft and hard tissues. The block sections were soaked in the same formalin solution and fixed in 70% ethanol, dehydrated in serial concentrations of ethanol, defatted in acetone, cleared with monomer, and then embedded in methyl methacrylate resin. After 3 weeks of polymerization at 35°C, the resin blocks were trimmed and cut. From each implant site, the middle portion of the implant and defect was precisely determined using X-ray analysis, and one central buccolingual section parallel to the long axis of the implant was carefully prepared with a micro-cutting machine (BS-3000, EXAKT®, Norderstedt, Germany) and was reduced to a thickness of about 20–25 µm and polished using a micro-griding machine (MG-400, EXAKT®, Norderstedt, Germany). The histological section was then stained in Villanueva Goldner stain and used for histological and histometrical analysis.

Histological and histometrical examinations

All histological sections were analyzed under a microscope (Eclipse E800, Nikon Inc., Tokyo, Japan) equipped with a computerized image system (Image-pro Plus™, Media Cybernectics, L.P., Silver Spring, MD, USA).

Before analysis, the distance (mm) of the implant shoulder to the bottom of the defect was measured using the clinical photographs which had been taken immediately after defect debridement (Fig. 5a). This distance was applied to determine the bottom of the bone defect after debridement (BBD), and consequently, the area of the bone defect in the histological sections in each implant for further histometric analysis. Also, the distances between the most coronal part of both the mesial (X_1) and distal (X_2) buccal alveolar crest of the bone defect and the bottom of the defect were measured in the photographs by a blinded examiner and the mean value of the both distances calculated. This mean value

represented the height of each original bone defect (HBD), and thereby, the position of coronal level of bone defect (CBD) was determined in each section. These BBD and CBD positions were used in further histometrical analysis. Then, the following landmarks were also identified in the histological sections: implant shoulder (IS); BBD; CBD; coronal level of newly formed bone originating from the old bone at the BBD (CNB).

For histometrical analysis, the following parameters were measured and calculated: new bone height (NBH), the distance between BBD and CNB; percent of NBH to HBD (%NBH); total length of implant surface within the original bone defect (LIS), the length of the threaded implant surface between BBD and CBD; total length of new bone-to-implant contact (NBIC), the length of the newly formed bone contacting the implant surface between BBD and CBD; percent of NBIC to LIS (%NBIC); new bone fill area (NBA), area of newly formed alveolar bone between BBD and CBD (Fig. 5b).

Statistical analysis

The mean value of the measurements of the two implants from the same group in each dog were calculated and used as a representative value of each animal. The mean and standard deviation for each histometric parameter were calculated for the laser and control groups. Differences between the groups were analyzed using Student *t*-test for paired observation ($n=4$). A p-value less than 0.05 was considered to indicate statistical significance.

Results

Bacterial detection

The bacterial detection by PCR revealed the presence of *P. gingivalis* and *T. forsythia* in the subgingival plaque sample after induction of peri-implant infection. However, *T. denticola*, *A. actinomycetemcomitans*, and *P. intermedia* were not detected (Fig. 6).

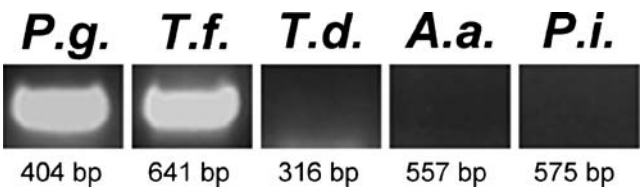

Fig. 6 Bacterial detection by polymerase chain reaction (PCR) analysis. The subgingival plaque was taken from the contaminated silk ligatures on the metal mesh after its removal from peri-implant pocket to examine the infection of five major periodontal pathogens. Electrophoresis results of PCR amplification (36 circles). The *numbers of base pairs* are shown for each specific bacterium. The DNA band shows the detection of *P. gingivalis* and *T. forsythia*

Clinical observations and treatment time

Before surgical treatment of the peri-implant infection, signs of gingival inflammation with bleeding on probing and pocket depth of approximately 5 mm were observed on the buccal site of the implant, which coincided with the mesiodistal center of the bone defect in all implants. After flap reflection, it was observed that the bone around the implant, adjacent to the defect, was resorbed to some extent, and all the bone defects were filled with diseased granulation tissue. Er:YAG laser irradiation achieved easily and effectively granulation tissue removal and implant surface debridement, while with plastic curet instrumentation, it was more difficult to perform the debridement compared to laser treatment (Table 1). In particular, the narrow space at the border between the bone and implant, and the implant surface between the threads, were more easily debrided by laser irradiation than plastic curet instrumentation. After laser treatment, no visible thermal damage such as carbonization was observed on the laser-treated bone or titanium implant surfaces, and more bleeding was noted from the treated bone defect compared to the curet-treated sites (Fig. 7b and d). Also, no mechanical damage such as scratches was visible on either the laser-treated or the curet-treated titanium surfaces (Fig. 7a and c).

With respect to the treatment time for debridement, the time of laser irradiation was 101.7±23.0 s and that of mechanical instrumentation was 215.7±70.4 s (mean ± SD, $n=8$). The laser therapy was significantly faster compared to the mechanical therapy ($p=0.004$) (Fig. 8).

During the healing phase, uneventful healing was observed for all of the laser and curet sites. Although 10 of 16 implant heads, 5 implants in the laser site and 5 implants in control site, were exposed during the course of wound healing, no visible adverse reactions such as swelling or suppuration occurred throughout the observation period.

Clinical measurements

Immediately after granulation tissue removal and implant surface debridement, the distance between the implant shoulder to the bottom of the defect (IS-BBD) was determined for all implants. The mean value calculated was 7.33±0.40 mm (mean ± SD, $n=8$) in the implants of the laser group and 7.14±0.25 mm (mean ± SD, $n=8$) in the control group. Also, the buccolingual thickness of the bone of the center at the bottom of the defect (TBBD) was determined. The mean value calculated was 1.44±0.37 mm (mean ± SD, $n=8$) in the laser group and 1.44±0.40 mm in the control

Table 1 Degree of difficulty of debridement for peri-implant bone defect and its implant surface and degree of bleeding from the bone defect after debridement

Dog no.	Degree of difficulty				Degree of bleeding			
	Laser		Curet		Laser		Curet	
	MI	DI	MI	DI	MI	DI	MI	DI
1	B	A	C	C	B	B	C	D
2	B	B	C	C	B	B	C	C
3	B	B	C	B	B	C	C	D
4	A	A	C	C	C	B	C	C

Degree of difficulty; *A* Very easy, *B* easy, *C* difficult, *D* impossible. Degree of bleeding; *A* Excessive, *B* moderate, *C* slight, and *D* no. *MI* Mesial implant, *DI* distal implant

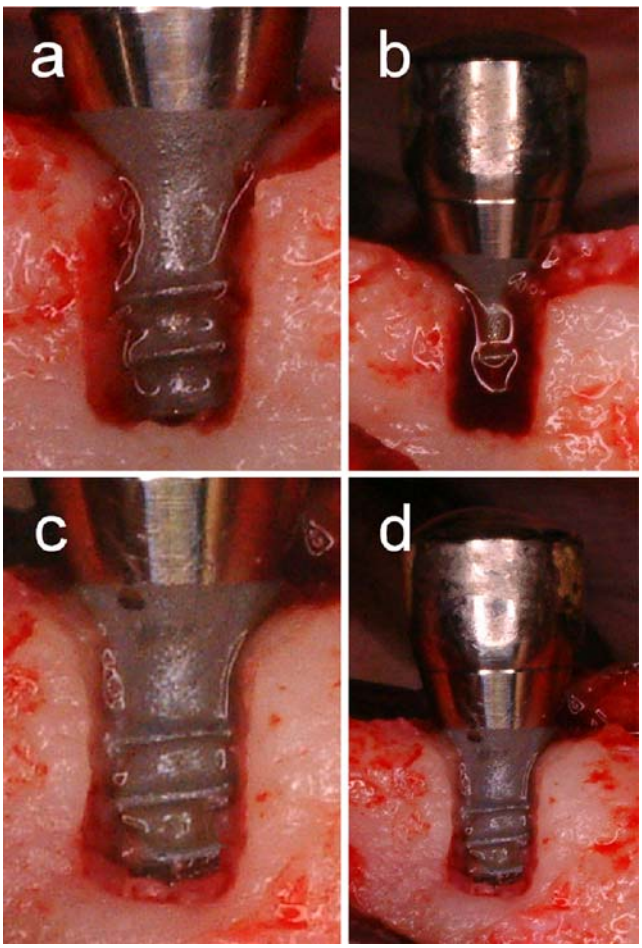

Fig. 7 Buccal view of the defects immediately after degranulation and implant surface debridement using an Er:YAG laser (**a**) or a plastic curet (**c**). Effective and safe granulation tissue removal and implant surface debridement with no macroscopically visible thermal damage were observed following Er:YAG laser irradiation of the implant surface and bone. Also, no visible mechanical injury was observed in the implants or bone treated by either of the procedures. The bleeding originating from the defect was removed to take the photograph. After debridement, a moderate amount of bleeding was generally observed from the bone defect in the laser-treated sites (**b**), different from the curet-treated sites, where generally no or substantially less bleeding was observed (**d**)

group. No statistical differences were observed in both parameters for either the position or dimension of bone defects after debridement (IS-BBD: $p=0.29$, BBDT: $p>0.99$).

Histological observations

All of the histological sections in the four animals were subjected to light microscopy. Two pairs of implants, one pair from dog no. 1 and another pair from dog no. 4, were excluded due to the mal-location of the mandibular nerve exposed at the bottom of the original bone defect, which interfered with new bone formation. Six pairs of implants in four dogs were subjected to histological analysis.

Three representative histological sections of each treatment group are shown in Fig. 9. Both the laser and control groups exhibited significant repair by new bone formation which was osseointegrated to the implant surface. The newly formed bone exhibited features of woven and lamellar bone, characterized by a trabecular pattern and marrow spaces with fibrovascular tissue. Although no structural differences of newly formed bone tissue were noted between the laser and control sites, the newly formed bone-to-implant contact displayed a more favorable condition with a longer distance of coronal extension from the

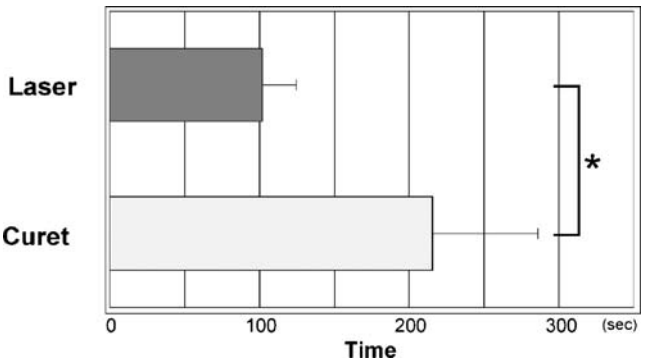

Fig. 8 Comparison of the time required for degranulation and implant surface debridement between the Er:YAG laser irradiation and plastic curet instrumentation. Data were expressed as the means ± SD (*$p<0.05$; Student *t*-test for paired observation $n=8$)

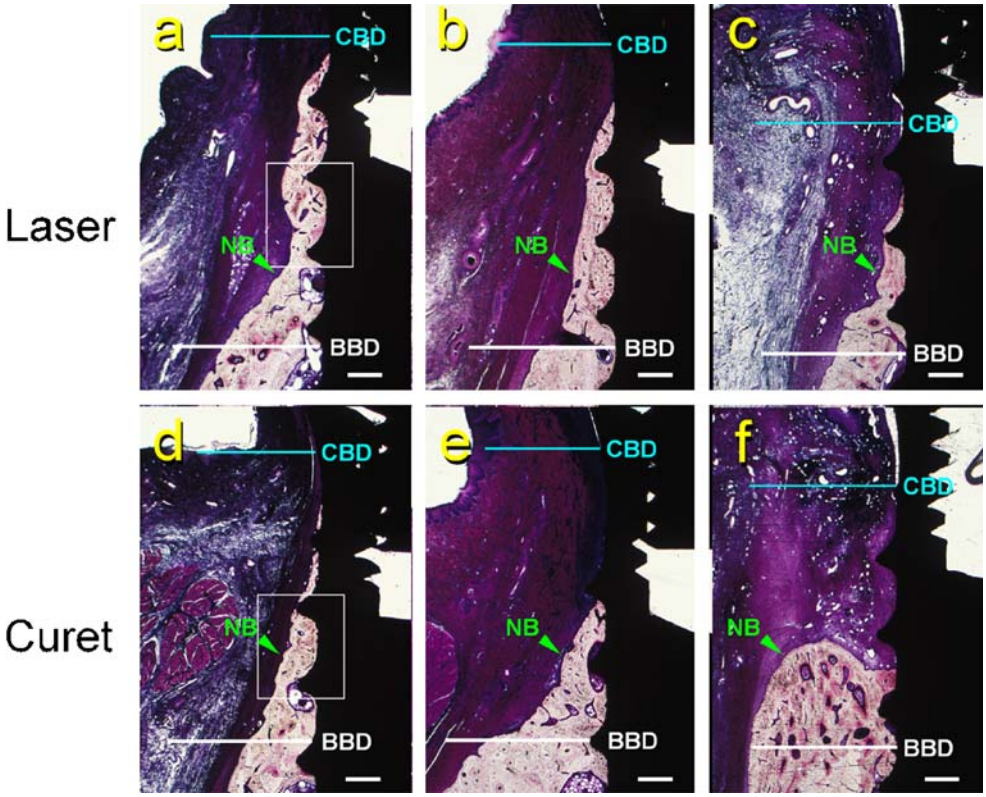

Fig. 9 Histological photomicrographs of the buccolingual non-decalcified sections parallel to the long axis of the implant in the center of the dehiscence defect at 24 weeks following degranulation and implant surface debridement in surgical therapy of peri-implant infection using an Er:YAG laser or a plastic curet. **a**, **d** Histological sections showing the highest new bone formation in the laser and control groups, respectively. **b**, **e** and **c**, **f** Two representative and typical paired sections of laser and control sites. In both the laser and plastic curet sites, some degree of new bone formation with no structural differences was noted in the defect area. In the laser group, the newly formed bone (NB) was more coronally extended along and in direct contact to the implant surface from the bottom of the bone defect (BBD) than the control. In the control group, only a small amount of new bone formation was in direct contact with the treated implant surface. (Villanueva Golder stain; *bar*=500 μm; original magnification ×30.) *CBD* Coronal level of bone defect

bottom in the laser sites than in the control sites. In the laser sites, five cases out of six had coronal new bone extension along the implant surface, which reached over half of original bone defect height, while in control sites, only two cases exhibited coronal extension. Regarding the implant surface, no major surface change of the original irregular microstructure was observed for both treatments under higher magnification and an intimate newly formed bone contact to the lased implant surface was observed (Fig. 10). Also in the laser group, no major thermal damage to the bone was observed without the presence of the affected layer on the bone which is usually produced immediately after laser irradiation. The interface between the original and newly formed bone following treatment was not always clearly detected due to the normal bone modeling and remodeling which takes place during the 6 months of healing process. However, in certain specimens, the original bottom position determined actually coincided with the distinguishable histological feature of the border between the old and new bone. In dog no. 1, in both the laser and curet treated-sites, isolated newly formed bone was present in direct contact with the treated implant surface but not connected with the bone from BBD, resulting in a low NBH.

Histometrical analysis

The mean height of original bone defect (HBD) judging from the clinical photographs and the mean length of implant surface within the original bone defect (LIS) measured in the histological sections were 3.91±0.48 and 4.76±0.57 mm (mean ± SD, n=6) in the laser group and 3.78±0.33 and 4.57±0.46 mm in the control group, respectively. No statistically significant differences were observed between the groups for HBD (p=0.62) and LIS

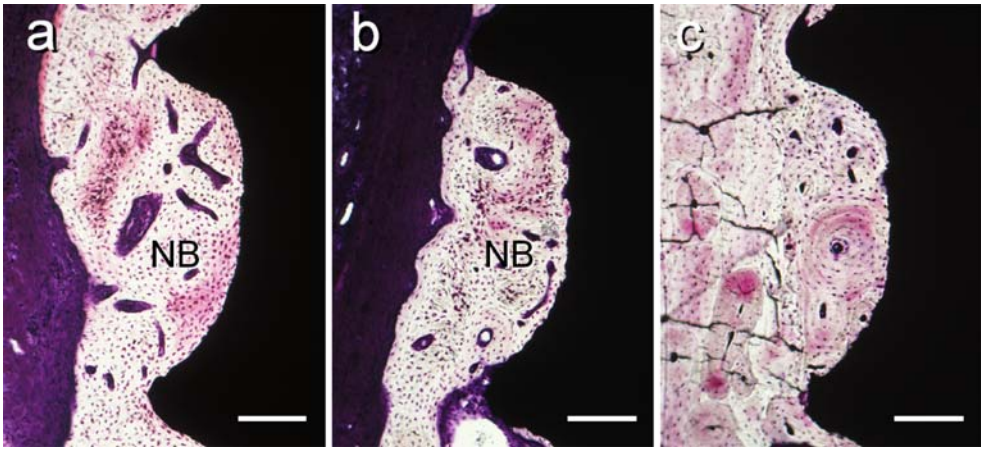

Fig. 10 Higher magnification of the area within the squares in Fig. 8a (**a**), 8d (**b**), and the area of bone contacting the intact implant surface (**c**). Note that direct contact was established between the newly formed bone and the treated implant surface in both the laser (**a**) and control (**b**) groups, similarly to the intact implant surface that shows a normal and usual osseointegration (**c**). The Er:YAG laser-treated implant surface did not inhibit the attachment and formation of new bone to its surface. (Villanueva Golder stain; *bar*=200 μm; original magnification ×100)

(p=0.45), showing that defects of both groups after debridement had similar dimensions. Regarding the histometrical analysis in two dogs (nos. 2 and 3), the mean of two implants in each group were used as a representative data for each dog, and consequently, four data points from four dogs were analyzed.

The mean percentage of new bone height (NBH) and new bone-to-implant contact (NBIC) were 61.8±32.7 and 69.7±15.2% (mean ± SD, n=4) in the laser group and 35.1±15.1 and 39.4±11.7% in the control group, respectively. A greater tendency of both NBH and NBIC were observed in the laser group, although the differences between groups did not reach the statistically significant level in either parameter (NBH p=0.11, NBIC p=0.08). The mean area of new bone (NBA) within the defect was 1.21±0.15 mm^2 (mean ± SD, n=4) in the laser group and 1.02±0.72 mm^2 in the control group (Fig. 11). A similar amount of new bone formation was achieved by both treatments (p=0.56). The values of each evaluated parameter in each dog are presented in Table 2.

Discussion

The elimination of the inflammatory lesion, the arrest of the disease progression, and the maintenance of the function with healthy peri-implant tissues are the primary goals in the treatment of peri-implantitis. To achieve the desired outcome, the removal of etiologic factors such as adherent plaque, bacterial deposits, and infected connective tissue within intrabony defects around the implants have all been cited as essential. However, conventional mechanical instruments such as steel curets or ultrasonic scalers are not completely suitable for granulation tissue removal and implant surface debridement because they readily damage the implant titanium surfaces [28], and thus, may interfere with the process of bone healing. Therefore, the implant

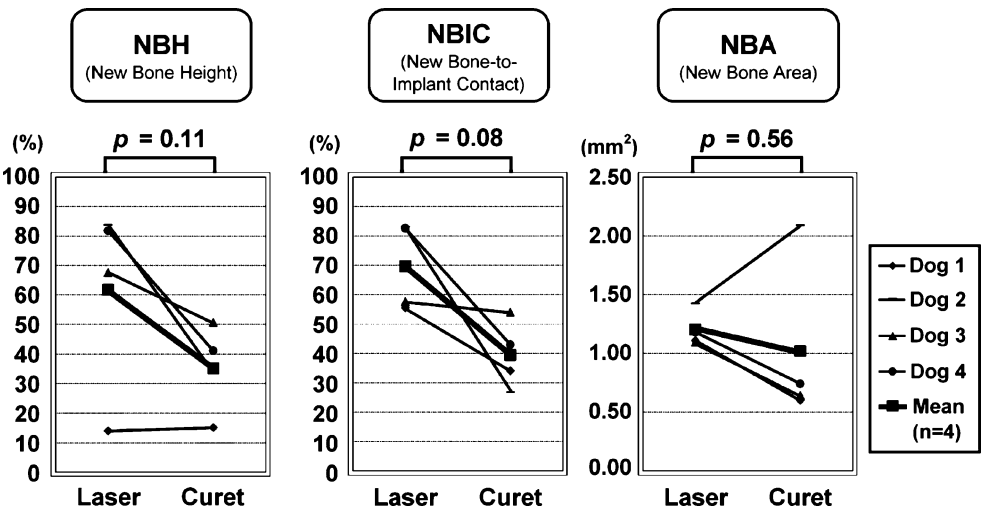

Fig. 11 Comparison of histometric analysis between the laser and control groups: new bone height (*NBH*), new bone-to-implant contact (*NBIC*), and new bone area (*NBA*). In *NBH* and *NBIC*, the measurement data obtained in millimeters were converted to a percentage relative to the height and length of implant surface of the bone defect following debridement. The data of NBA is shown in square millimeters. The *thick line* shows the mean in each graph (Student *t*-test for paired observation n=4)

Table 2 Histometrical measurements of NBH, NBIC, and NBA in both the laser and control group of each dog

Dog No.	Percent NBH (%)		Percent NBIC (%)		NBA (mm^2)	
	Laser	Curet	Laser	Curet	Laser	Curet
1	13.9	15.1	55.5	34.0	1.11	0.60
2	83.8	33.4	83.1	26.8	1.43	2.09
3	67.7	50.8	57.6	53.9	1.10	0.65
4	81.8	41.1	82.6	42.9	1.18	0.74
Mean ± SD	61.8±32.7	35.1±15.1	69.7±15.2	39.4±11.7	1.21±0.15	1.02±0.72

debridement is usually performed by mechanical means such as plastic curets and carbon fiber curets [12–14, 29, 30]. However, these methods are apparently ineffective for complete debridement of the bone defect and the contaminated implant surface [30–33], and also, the mechanical debridement is not easy and is time-consuming. Furthermore, recently, implants with microstructured surface have been clinically employed, as the rough surface improves anchorage force to alveolar bone [34]. Accordingly, in the case of peri-implantitis, complete removal of contaminants such as bacteria and their products, and soft tissue cells from the rough surface, has become much more difficult with mechanical debridement [30, 32, 33], and the remaining plaque biofilm might interfere with the healing of the peri-implant tissues. Therefore, the use of adjunctive chemical agents such as irrigation or polishing with local disinfectants and local or systemic antibiotic therapy have been performed with considerable success following mechanical procedure in the clinic [12, 14, 35], although the emergence of bacterial resistance to antibiotics owing to frequent doses of antibiotics is a matter of concern. There is significant interest in the development of an alternative antimicrobial treatment modality.

Recently, a great deal of attention has been focused on novel therapeutic methods using lasers. Lasers have been applied as an adjunctive or alternative treatment in peri-implant therapy and are expected to resolve the difficulties and problems of the conventional mechanical treatment. Among the lasers applied in dentistry, the Er:YAG laser is considered to possess excellent properties for both degranulation and implant surface decontamination in the treatment of peri-implantitis. Clinical studies have already reported that the application of the Er:YAG laser for nonsurgical treatment of peri-implantitis led to significant clinical improvements 6 months after therapy [12, 13]. Regarding histological examination, only one study has reported that the Er:YAG laser surgery seems to be more suitable to promote re-osseointegration than plastic curet instrumentation followed by subgingival application of an antibiotic agent for the treatment of peri-implantitis in a circumferential crater-like bone defect [14]. However, further histological studies using different models of peri-implantitis and different irradiation parameters are necessary to minutely elucidate the various effects of the Er:YAG laser. Also, a direct comparison of implant debridement effectiveness between the Er:YAG laser and mechanical treatment alone is required. Therefore, in the present study, localized peri-implant infection with a buccal dehiscence-type bone defect was experimentally prepared, and Er:YAG laser treatment was performed.

Experimental induction of peri-implant infection

The commonly utilized animal model of experimental peri-implantitis has been the ligature-induced peri-implantitis previously described by Lindhe et al. [36]. In this model, cotton ligatures are placed in a submarginal position around the neck of the implants, allowing submarginal plaque accumulation and subsequent loss of supporting bone, resulting in the production of a circumferential-type bone defect. This model of peri-implantitis is easily produced, but it is difficult to obtain a sufficient vertical dimension for bone regeneration on the treated implant surface without the employment of regenerative procedures. In the present study, an original, unique model of experimental localized peri-implant infection with relatively the same dimensions of bone defect were prepared, which was induced by placement of stainless steel mesh sheet with a silk ligature for an accumulation of supra and subgingival plaque in surgically created buccal dehiscence-type bone defect around an implant, resulting in the formation of submarginal bacterial deposits and diseased granulation tissues. Although this model required many steps and a long period for preparation, the bone defect obtained was simple, unified, and suitable to induce sufficient vertical dimension of new bone formation. In the circumferential-type bone defects, the vertical new bone formation is limited, and usually, the presence of a dense connective tissue is observed between the newly formed bone to the treated-implant surface, making the evaluation of the biocompatibility of the treated-implant surface difficult. In contrast, the model applied in the present study was advantageous to evaluate the biocompatibility of the lased-treated implant surface on the formation of the newly formed bone, as in

this dehiscence-type bone defect, a sufficient vertical bone gain with an intimate contact to implant surface is expected without the application of regenerative therapy procedures [37]. However, it should be pointed out that in this model, the exposed implant surface in the dehiscence bone defect was not previously osseointegrated, and consequently, the osseointegration after treatment does not precisely show the "re-osseointegration" process per se. Also, animals with bucco-lingual thick mandible should be employed to prevent the interference of new bone formation by the mandibular nerve in this model.

Regarding the microbial infection, the bacterial detection by PCR analysis of the submarginal dental plaque revealed the infection of peri-implant pocket by periodontopathic bacteria such as *P. gingivalis* and *T. forsythia* which are major bacteria associated with periodontitis and peri-implantitis in human [7, 8]. Therefore, it was confirmed that the peri-implant infection prepared in the present study was microbiologically similar to the peri-implant infection in humans.

Granulation tissue removal and implant surface debridement

Thorough degranulation is important in the treatment of periodontal and peri-implant bone defects, as the residual diseased granulation tissue, which contains pathogenic bacteria [38] and substantially increased levels of inflammatory cytokines and mediators [39], could negatively affect new bone formation. Regarding the ability of lasers for degranulation, Williams et al. [40] reported an efficient ablation of periodontal granulation tissue with a carbon dioxide (CO_2) laser in dogs. However, the study demonstrated that the CO_2 laser produced carbonization on the bone surface. In contrast, Mizutani at al. [6] demonstrated an effective granulation tissue removal by Er:YAG laser in a furcation bone defect of experimentally induced periodontitis in dogs, without causing major thermal damage to the bone and root surfaces. Clinically, Schwarz et al. [41], and Sculean et al. [42] have already demonstrated effective granulation tissue removal from periodontal bone defects using an Er:YAG laser during periodontal flap surgery and significant clinical improvement 6 months postsurgery. Thus, the effectiveness of this laser for degranulation in periodontal therapy has already been shown, and therefore, an effective removal of granulation tissue in peri-implant bone defects was expected.

In the present study, the Er:YAG laser irradiation, achieved safe, effective, and thorough granulation tissue removal and implant surface debridement without any macroscopically visible thermal damage such as carbonization or melting on the laser-treated bone and implant surfaces. Regarding the time required for treatment, the Er:YAG laser treatment was shown faster than conventional hand instrumentation using a curet, as the chisel-type tip utilized was well adapted to the buccal dehiscence bone defect and could easily ablate the granulation tissue which clung to the bone surface. Although the conditions of present animal study may not be directly applied to the clinical situation, the present histological findings suggest that the Er:YAG laser is a promising tool for degranulation and implant surface debridement.

Effect of Er:YAG laser on titanium implant

In the present study, the histological sections revealed the intimate contact of the newly formed bone to the Er:YAG laser-treated implant surface. The majority of implants treated with Er:YAG laser exhibited greater NBIC and favorable bone healing than those treated by the curet. The findings may be partly attributed to the superior decontamination and detoxification effect of the Er:YAG laser, unlike the plastic curet treatment that does not evidently achieve complete implant surface decontamination [32, 33].

Some types of lasers are unsuitable for implant surface treatment, as morphological changes such as cracks, melting, and crater formation of the titanium surface have been observed following neodymium-doped:YAG (Nd:YAG) and holmium-doped:YAG laser irradiation [43]. With the CO_2 laser, no morphological changes on the implant surface were reported following the irradiation, and this laser is commonly applied for decontamination of implant surfaces [44]. However, there is a risk associated with the high temperature elevation of the titanium implant surface and adjacent bone tissue during CO_2 laser irradiation [45, 46]. In the present study, no macroscopically visible thermal or mechanical damage was observed on the implant surface following Er:YAG laser irradiation at 10 J/cm^2 per pulse and 20 Hz with water spray. Matsuyama et al. [17] reported that Er:YAG laser irradiation did not cause any visible surface changes of titanium under 50 mJ/pulse (energy density 17.7 J/ cm^2) with the use of water spray in near contact mode. Furthermore, Schwarz et al. [47] demonstrated that no alterations were detectable in any of the investigated microstructural surface patterns of implants irradiated at energy densities of 12.7 J/cm^2 and 10 Hz with water cooling. Thus, the Er:YAG laser may be accepted for implant surface debridement within a suitable energy level range. Recently, higher pulse repetition rates have become available, and this might increase the risk of thermal damage of the titanium implant surface. However, in the present study, which employed a higher pulse rate of 20 Hz, the Er:YAG laser-treated implant surface did not clinically interfere with the healing and attachment of the newly formed bone to the laser-treated implant surface.

New bone formation after treatment

Under the conditions of this study, the Er:YAG laser did not elicit any adverse effects on the healing of bone. The affected layer, which is a thin layer with thermal and structural changes and is usually produced on irradiated hard tissues by Er:YAG laser ablation [3, 48–50], was not detected on the interface between the old and newly formed bone. This finding is in accordance with our previous study [6], which demonstrated that this affected layer was scarcely detectable on the irradiated bone tissue following 12 weeks of healing after periodontal surgery using an Er:YAG laser. It is considered that the affected layer was resorbed by bone remodeling during the healing phase.

Regarding new bone formation, significant amounts of newly formed bone of various degrees were observed in both the laser and curet sites after 24 weeks of healing. The mean value of NBA was similar in both groups. However, the pattern of new bone formation seemed different between the laser and curet sites. The newly formed bone in the laser sites was more coronally extended in direct contact along the implant surface than that in the curet sites, and therefore, the laser group showed greater mean values for both NBH and NBIC than the control group.

Regarding the promotion of new bone formation, it has been reported that the CO_2 laser possess an ability to enhance bone regeneration when utilized for decontamination of implants in the treatment of experimentally induced peri-implantitis [16]. Similar to our previous study [6] which showed greater new bone formation in the Er:YAG laser-treated sites than curet-treated sites after surgical treatment of periodontitis, the following positive effects could be considered as reasons for greater NBH and greater NBIC: thorough granulation tissue removal with high decontamination of both bone and implant surfaces [6, 15], more pronounced bleeding originating from the bone defect following debridement, the microstructural topography of bone tissue following laser irradiation which is advantageous for blood clot retention [51], and the suggested biostimulatory effect promoting new bone formation [52, 53]. In addition, the specific characteristics of the titanium surface also seem to be decisive for the healing of the bone. The level of NBIC is reported to be significantly increased by implant surface roughness [11, 54], and Er:YAG laser is capable of performing detoxification and decontamination of the SLA implant surface [15, 55]. In the present study, the Er:YAG laser treatment induced more bleeding, which may be due to the low thermal effect of the Er:YAG laser and the slightly porous bone surface without a smear layer treated by Er:YAG. Bleeding from bone marrow has been previously demonstrated to promote new bone formation [56]. In this context, in the laser site, more pronounced bleeding from the bone marrow immediately after treatment, in conjunction with the shape of bone defect employed which was advantageous for the blood clot formation after bleeding, resulted in increased blood clot formation, and the Er:YAG laser-treated SLA implant surface might have provided beneficial conditions for cell attachment and the retention and stability of the blood clot that forms in the bone defect.

Schwarz et al. [14] reported that no statistically significant differences of bone regeneration were observed between the experimentally induced peri-implantitis sites in dogs treated by Er:YAG laser irradiation alone and the plastic curet in conjunction with application of metranidazole gel 25%. However, both NBIC and NBH in their study did exhibited higher mean values in the laser-treated group than the mechanically treated group. Therefore, considering the results of the present study in combination with those of their study, Er:YAG laser seems to possess a higher decontamination effect and to induce more osseointegration than conventional mechanical instrumentation [14].

In the present study, the difference in the histological results between the two treatments was not statistically significant, which may be due to the biological variability of the animals in association with the small sample size. It should be pointed out that in the present study, the number of experimental animals used was limited and further studies with larger sample size are necessary. However, nevertheless, the greater tendency of NBH and NBIC in the laser group than the curet group demonstrates that the Er:YAG laser has promise as a tool in the surgical treatment of peri-implantitis. Further investigations should be also carried out to minutely examine the effect of Er:YAG laser therapy in combination with regenerative procedures in the treatment of peri-implantitis.

Conclusion

Under the conditions of the present study, it may be concluded that the Er:YAG laser can be safely and effectively utilized for degranulation and implant surface debridement in the surgical treatment of peri-implant infection. Based on the histological results, both treatments showed significant new bone formation on the treated implant surface. Noticeably, the laser-treated group showed a favorable tendency to produce greater new bone height and new bone-to-implant contact than the curet-treated surface, although the difference was not statistically significant. The energy parameters applied in this laser study did not result in any deleterious thermal damage to the bone or the implant surfaces. Treatment of peri-implantitis by Er:YAG laser irradiation holds promise and seems to be more effective than mechanical treatment alone.

Acknowledgments This study was supported, in part, by the grant for 21st Century Center of Excellence Program for Frontier Research on Molecular Destruction and Reconstruction of Tooth and Bone in Tokyo Medical and Dental University and by a Grant-in-Aid for Scientific Research(c)(2) (No. 16592064) (A.A.), Ministry of Education, Culture, Sports, Science and Technology of Japan. The laser apparatus was provided by the HOYA Conbio Corp. (Fremont, CA, USA). Authors wish to thank Drs. Atsuhiro Kinoshita, Tatsuya Akizuki, Chie Hayashi, Kosuke Tanaka, Ikufumi Sato, and Hiroaki Maruyama for their kind technical advice and support.

References

1. Hale GM, Querry MR (1973) Optical constants of water in the 200-nm to 200-m wavelength region. Appl Opt 12:555–563
2. Aoki A, Ando Y, Watanabe H, Ishikawa I (1994) In vitro studies on laser scaling of subgingival calculus with an erbium:YAG laser. J Periodontol 65:1097–1106
3. Aoki A, Miura M, Akiyama F, Nakagawa N, Tanaka J, Oda S, Watanabe H, Ishikawa I (2000) In vitro evaluation of Er:YAG laser scaling of subgingival calculus in comparison with ultrasonic scaling. J Periodontal Res 35:266–277
4. Schwarz F, Putz N, Georg T, Reich E (2001) Effect of an Er:YAG laser on periodontally involved root surfaces: an in vivo and in vitro SEM comparison. Lasers Surg Med 29:328–335
5. Schwarz F, Sculean A, Berakdar M, Szathmari L, Georg T, Becker J (2003) In vivo and in vitro effects of an Er:YAG laser, a GaAlAs diode laser, and scaling and root planing on periodontally diseased root surfaces: a comparative histologic study. Lasers Surg Med 32:359–366
6. Mizutani K, Aoki A, Takasaki AA, Kinoshita A, Hayashi C, Oda S, Ishikawa I (2006) Periodontal tissue healing following flap surgery using an Er:YAG laser in dogs. Lasers Surg Med 38:314–324
7. Mombelli A, van Oosten MA, Schurch E, Jr., Land NP (1987) The microbiota associated with successful or failing osseointegrated titanium implants. Oral Microbiol Immunol 2:145–151
8. Listgarten MA, Lai CH (1999) Comparative microbiological characteristics of failing implants and periodontally diseased teeth. J Periodontol 70:431–437
9. Persson LG, Araujo MG, Berglundh T, Grondahl K, Lindhe J (1999) Resolution of peri-implantitis following treatment. An experimental study in the dog. Clin Oral Implants Res 10:195–203
10. Wetzel AC, Vlassis J, Caffesse RG, Hammerle CH, Lang NP (1999) Attempts to obtain re-osseointegration following experimental peri-implantitis in dogs. Clin Oral Implants Res 10:111–119
11. Persson LG, Berglundh T, Lindhe J, Sennerby L (2001) Re-osseointegration after treatment of peri-implantitis at different implant surfaces. An experimental study in the dog. Clin Oral Implants Res 12:595–603
12. Schwarz F, Sculean A, Rothamel D, Schwenzer K, Georg T, Becker J (2005) Clinical evaluation of an Er:YAG laser for nonsurgical treatment of peri-implantitis: a pilot study. Clin Oral Implants Res 16:44–52
13. Schwarz F, Bieling K, Nuesry E, Sculean A, Becker J (2006) Clinical and histological healing pattern of peri-implantitis lesions following non-surgical treatment with an Er:YAG laser. Lasers Surg Med 38:663–671
14. Schwarz F, Jepsen S, Herten M, Sager M, Rothamel D, Becker J (2006) Influence of different treatment approaches on non-submerged and submerged healing of ligature induced peri-implantitis lesions: an experimental study in dogs. J Clin Periodontol 33:584–595
15. Kreisler M, Kohnen W, Christoffers AB, Gotz H, Jansen B, Duschner H, d'Hoedt B (2005) In vitro evaluation of the biocompatibility of contaminated implant surfaces treated with an Er:YAG laser and an air powder system. Clin Oral Implants Res 16:36–43
16. Stubinger S, Henke J, Donath K, Deppe H (2005) Bone regeneration after peri-implant care with the CO_2 laser: a fluorescence microscopy study. Int J Oral Maxillofac Implants 20:203–210
17. Matsuyama T, Aoki A, Oda S, Yoneyama T, Ishikawa I (2003) Effects of the Er:YAG laser irradiation on titanium implant materials and contaminated implant abutment surfaces. J Clin Laser Med Surg 21:7–17
18. Sasaki KM, Aoki A, Masuno H, Ichinose S, Yamada S, Ishikawa I (2002) Compositional analysis of root cementum and dentin after Er:YAG laser irradiation compared with CO_2 lased and intact roots using Fourier transformed infrared spectroscopy. J Periodontal Res 37:50–59
19. Sasaki KM, Aoki A, Ichinose S, Ishikawa I (2002) Morphological analysis of cementum and root dentin after Er:YAG laser irradiation. Lasers Surg Med 31:79–85
20. Ando Y, Aoki A, Watanabe H, Ishikawa I (1996) Bactericidal effect of erbium YAG laser on periodontopathic bacteria. Lasers Surg Med 19:190–200
21. Folwaczny M, Mehl A, Aggstaller H, Hickel R (2002) Antimicrobial effects of 2.94 micron Er:YAG laser radiation on root surfaces: an in vitro study. J Clin Periodontol 29:73–78
22. Schwarz F, Aoki A, Sculean A, Georg T, Scherbaum W, Becker J (2003) In vivo effects of an Er:YAG laser, an ultrasonic system and scaling and root planing on the biocompatibility of periodontally diseased root surfaces in cultures of human PDL fibroblasts. Lasers Surg Med 33:140–147
23. Yamaguchi H, Kobayashi K, Osada R, Sakuraba E, Nomura T, Arai T, Nakamura J (1997) Effects of irradiation of an erbium: YAG laser on root surfaces. J Periodontol 68:1151–1155
24. Aoki A, Sasaki KM, Watanabe H, Ishikawa I (2004) Lasers in nonsurgical periodontal therapy. Periodontol 2000 36:59–97
25. Ishikawa I, Aoki A, Takasaki AA (2004) Potential applications of Erbium:YAG laser in periodontics. J Periodontal Res 39:275–285
26. Takasaki AA, Aoki A, Ishikawa I (2006) Erbium:YAG laser in Periodontics. Dent Jpn 42:200–206
27. Ashimoto A, Chen C, Bakker I, Slots J (1996) Polymerase chain reaction detection of 8 putative periodontal pathogens in subgingival plaque of gingivitis and advanced periodontitis lesions. Oral Microbiol Immunol 11:266–273
28. Fox SC, Moriarty JD, Kusy RP (1990) The effects of scaling a titanium implant surface with metal and plastic instruments: an in vitro study. J Periodontol 61:485–490
29. Shibli JA, Martins MC, Nociti FH, Jr., Garcia VG, Marcantonio E, Jr. (2003) Treatment of ligature-induced peri-implantitis by lethal photosensitization and guided bone regeneration: a preliminary histologic study in dogs. J Periodontol 74:338–345
30. Karring ES, Stavropoulos A, Ellegaard B, Karring T (2005) Treatment of peri-implantitis by the Vector system. Clin Oral Implants Res 16:288–293
31. Augthun M, Tinschert J, Huber A (1998) In vitro studies on the effect of cleaning methods on different implant surfaces. J Periodontol 69:857–864
32. Schwarz F, Sculean A, Romanos G, Herten M, Horn N, Scherbaum W, Becker J (2005) Influence of different treatment approaches on the removal of early plaque biofilms and the viability of SAOS2 osteoblasts grown on titanium implants. Clin Oral Investig 9:111–117
33. Schwarz F, Papanicolau P, Rothamel D, Beck B, Herten M, Becker J (2006) Influence of plaque biofilm removal on

reestablishment of the biocompatibility of contaminated titanium surfaces. J Biomed Mater Res A 77:437–444
34. Carlsson L, Rostlund T, Albrektsson B, Albrektsson T (1988) Removal torques for polished and rough titanium implants. Int J Oral Maxillofac Implants 3:21–24
35. Roos-Jansaker AM, Renvert S, Egelberg J (2003) Treatment of peri-implant infections: a literature review. J Clin Periodontol 30:467–485
36. Lindhe J, Berglundh T, Ericsson I, Liljenberg B, Marinello C (1992) Experimental breakdown of peri-implant and periodontal tissues. A study in the beagle dog. Clin Oral Implants Res 3:9–16
37. Hanisch O, Sorensen RG, Kinoshita A, Spiekermann H, Wozney JM, Wikesjo UM (2003) Effect of recombinant human bone morphogenetic protein-2 in dehiscence defects with non-submerged immediate implants: an experimental study in Cynomolgus monkeys. J Periodontol 74:648–657
38. Liakoni H, Barber P, Newman HN (1987) Bacterial penetration of pocket soft tissues in chronic adult and juvenile periodontitis cases. An ultrastructural study. J Clin Periodontol 14:22–28
39. Dongari-Bagtzoglou AI, Warren WD, Berton MT, Ebersole JL (1997) CD40 expression by gingival fibroblasts: correlation of phenotype with function. Int Immunol 9:1233–1241
40. Williams TM, Cobb CM, Rapley JW, Killoy WJ (1995) Histologic evaluation of alveolar bone following CO_2 laser removal of connective tissue from periodontal defects. Int J Periodontics Restor Dent 15:497–506
41. Schwarz F, Sculean A, Georg T, Becker J (2003) Clinical evaluation of the Er:YAG laser in combination with an enamel matrix protein derivative for the treatment of intrabony periodontal defects: a pilot study. J Clin Periodontol 30:975–981
42. Sculean A, Schwarz F, Berakdar M, Windisch P, Arweiler NB, Romanos GE (2004) Healing of intrabony defects following surgical treatment with or without an Er:YAG laser. J Clin Periodontol 31:604–608
43. Kreisler M, Gotz H, Duschner H (2002) Effect of Nd:YAG, Ho:YAG, Er:YAG, CO2, and GaAIAs laser irradiation on surface properties of endosseous dental implants. Int J Oral Maxillofac Implants 17:202–211
44. Kato T, Kusakari H, Hoshino E (1998) Bactericidal efficacy of carbon dioxide laser against bacteria-contaminated titanium implant and subsequent cellular adhesion to irradiated area. Lasers Surg Med 23:299–309
45. Oyster DK, Parker WB, Gher ME (1995) CO_2 lasers and temperature changes of titanium implants. J Periodontol 66:1017–1024
46. Mouhyi J, Sennerby L, Nammour S, Guillaume P, Van Reck J (1999) Temperature increases during surface decontamination of titanium implants using CO_2 laser. Clin Oral Implants Res 10:54–61
47. Schwarz F, Rothamel D, Sculean A, Georg T, Scherbaum W, Becker J (2003) Effects of an Er:YAG laser and the vector ultrasonic system on the biocompatibility of titanium implants in cultures of human osteoblast-like cells. Clin Oral Implants Res 14:784–792
48. Nelson JS, Yow L, Liaw LH, Macleay L, Zavar RB, Orenstein A, Wright WH, Andrews JJ, Berns MW (1988) Ablation of bone and methacrylate by a prototype mid-infrared erbium:YAG laser. Lasers Surg Med 8:494–500
49. Aoki A, Ishikawa I, Yamada T, Otsuki M, Watanabe H, Tagami J, Ando Y, Yamamoto H (1998) Comparison between Er:YAG laser and conventional technique for root caries treatment in vitro. J Dent Res 77:1404–1414
50. Sasaki KM, Aoki A, Ichinose S, Ishikawa I (2002) Ultrastructural analysis of bone tissue irradiated by Er:YAG Laser. Lasers Surg Med 31:322–332
51. Sasaki KM, Aoki A, Ichinose S, Yoshino T, Yamada S, Ishikawa I (2002) Scanning electron microscopy and Fourier transformed infrared spectroscopy analysis of bone removal using Er:YAG and CO_2 lasers. J Periodontol 73:643–652
52. Dortbudak O, Haas R, Mallath-Pokorny G (2000) Biostimulation of bone marrow cells with a diode soft laser. Clin Oral Implants Res 11:540–545
53. Ninomiya T, Miyamoto Y, Ito T, Yamashita A, Wakita M, Nishisaka T (2003) High-intensity pulsed laser irradiation accelerates bone formation in metaphyseal trabecular bone in rat femur. J Bone Miner Metab 21:67–73
54. Botticelli D, Berglundh T, Persson LG, Lindhe J (2005) Bone regeneration at implants with turned or rough surfaces in self-contained defects. An experimental study in the dog. J Clin Periodontol 32:448–455
55. Friedmann A, Antic L, Bernimoulin JP, Purucker P (2006) In vitro attachment of osteoblasts on contaminated rough titanium surfaces treated by Er:YAG laser. J Biomed Mater Res A 79:53–60
56. Alberius P, Gordh M, Lindberg L, Johnell O (1996) Effect of cortical perforations of both graft and host bed on onlay incorporation to the rat skull. Eur J Oral Sci 104:554–561